Frontiers in Bioscience Landmark

Front. Biosci. (Landmark Ed) **2026**; 31(11): 57166
https://doi.org/10.31083/FBL57166

Original Research

Nifuroxazide Ameliorates Bisphenol A-Induced Cardiotoxicity in Rats via Suppression of TLR-4/NF-κB Signaling and Activation of the SIRT1/Nrf2/HO-1 Pathway

Reem N. Alotaibi[1], Emad H.M. Hassanein[2], Afnan Bakhsh[3], Amal A. Albati[1], Sulaiman M. Alnasser[4], Ashwaq H. Batawi[5], Mohamed A. Elsawy[6], Ayman M. Mahmoud[7,*]

[1]Biochemistry Department, College of Science, King Saud University, 11495 Riyadh, Saudi Arabia
[2]Department of Pharmacology and Toxicology, Faculty of Pharmacy, Al-Azhar University, 71524 Assiut, Egypt
[3]Department of Clinical Laboratory Sciences, College of Applied Medical Sciences, King Saud University, 11433 Riyadh, Saudi Arabia
[4]Department of Pharmacology and Toxicology, College of Pharmacy, Qassim University, 52571 Buraydah, Saudi Arabia
[5]Department of Biological Science, Faculty of Science, King Abdulaziz University, 21589 Jeddah, Saudi Arabia
[6]Division of Pharmacy and Optometry, School of Health Sciences, University of Manchester, M13 9PT Manchester, UK
[7]School of Biological and Chemical Sciences, Faculty of Science and Engineering, Manchester Metropolitan University, M1 5GD Manchester, UK
*Correspondence: a.mahmoud@mmu.ac.uk (Ayman M. Mahmoud)

Academic Editors: Piergiorgio La Rosa and Vesna Jacevic
Submitted: 17 August 2026 Revised: 13 October 2026 Accepted: 28 October 2026 Published: 18 November 2026

Abstract

Background: Bisphenol A (BPA) is a widespread environmental contaminant and endocrine disruptor that poses significant risks to cardiovascular health. Oxidative stress and chronic inflammation are key processes in the toxicity of BPA. This study aimed to evaluate the cardioprotective efficacy of nifuroxazide (NFZ), an antibacterial drug with promising antioxidant properties, against BPA-induced cardiotoxicity in rats, pointing to the involvement of the toll-like receptor 4 (TLR-4)/nuclear factor-kappaB (NF-κB) and sirtuin 1 (SIRT1)/nuclear factor erythroid 2-related factor 2 (Nrf2)/heme oxygenase-1 (HO-1) signaling, along with the adaptive regulators hypoxia-inducible factor (HIF)-1α and thioredoxin reductase 1 (TXNRD1). **Methods:** Male Wistar rats were divided into four groups: Control, NFZ (50 mg/kg), BPA (25 mg/kg), and BPA + NFZ. After four weeks of oral administration, cardiac injury was assessed via serum biomarkers, and myocardial tissue was analyzed for oxidative status, inflammatory markers, and histopathological changes. **Results:** BPA exposure resulted in significant cardiac injury, characterized by elevated serum cardiac troponin I (cTnI), creatine kinase MB (CK-MB), and lactate dehydrogenase (LDH), alongside histopathological alterations and myocardial fibrosis. These effects were accompanied by increased lipid peroxidation, decreased reduced glutathione (GSH), superoxide dismutase (SOD) and catalase, upregulated TLR-4, NF-κB, tumor necrosis factor (TNF)-α, and interleukin (IL)-1β. Furthermore, BPA downregulated SIRT1, Nrf2, HIF-1α, and TXNRD1 and suppressed HO-1 activity. NFZ effectively reversed these biochemical and structural abnormalities, suppressed TLR-4, NF-κB, TNF-α, and IL-1β, boosted antioxidants, and restored SIRT1, Nrf2, HO-1, HIF-1α, and TXNRD1. Molecular docking predicted favorable interactions of BPA with SIRT1, HO-1, and TXNRD1, including overlap with binding residues of their respective reference ligands. **Conclusion:** NFZ confers significant protection against BPA-induced cardiotoxicity. This protective activity is associated with restoration of redox homeostasis and alleviation of TLR-4/NF-κB and SIRT1/Nrf2/HO-1 signaling, suggesting its potential as a promising protective agent against BPA-induced cardiac injury.

Keywords: bisphenol A; nifuroxazide; cardiotoxicity; oxidative stress; inflammation

1. Introduction

Bisphenol A (BPA) is a synthetic organic compound widely utilized primarily in the industry of polycarbonate plastics and epoxy resins. These materials are widespread in modern society, found in food and beverage containers, thermal papers, dental sealants, and various medical devices [1,2]. Consequently, human exposure to BPA is virtually continuous and largely unavoidable, occurring through multiple routes including dietary intake, dermal absorption, and inhalation of contaminated dust [2,3,4]. While dietary intake is generally considered the predominant source, non-dietary routes, particularly dermal and inhalation, can lead to greater systemic availability of unconjugated, biologically active BPA. This results in a longer circulatory half-life for active BPA compared to orally absorbed BPA [5]. BPA functions as a well-recognized xenoestrogen and endocrine-disrupting chemical (EDC) due to its structural resemblance to 17β-estradiol. Therefore, it exerts profound adverse effects on diverse physiological systems by interfering with hormonal signaling [6]. Beyond its well-documented estrogenic activities, BPA toxicity manifests as reproductive dysfunction, metabolic disturbances, neurobehavioral deficits, and detrimental effects on vital organs such as the liver, kidney, and heart [7,8,9,10].

Copyright: © 2026 The Author(s). Published by IMR Press.
This is an open access article under the CC BY 4.0 license.

Publisher's Note: IMR Press stays neutral with regard to jurisdictional claims in published maps and institutional affiliations.

BPA-induced cardiotoxicity has emerged as an important public health concern owing to the widespread human exposure and its growing association with adverse cardiovascular outcomes [10]. Epidemiological investigations have consistently demonstrated a correlation between elevated urinary BPA concentrations and an increased risk of cardiovascular disorders, including arrhythmias, hypertension, atherosclerosis, myocardial infarction, and heart failure [11]. This impact of BPA on the cardiovascular system was corroborated by experimental studies showing its disruptive effects on calcium homeostasis, ion channel activity, and cardiac electrophysiology [12,13,14]. Regarding the mechanism underlying BPA toxicity, oxidative stress and inflammation have been identified as key players [15,16]. BPA promotes excessive generation of reactive oxygen species (ROS) via its redox cycling, resulting in oxidative stress characterized by depletion of endogenous antioxidants [15]. The resulting oxidative burden promotes lipid peroxidation (LPO), destabilizes cellular membranes, and causes oxidative modification of proteins and nucleic acids, thereby compromising cardiomyocyte viability and contributing to the progression of myocardial injury [17]. In addition to their direct cytotoxic effects, ROS function as important intracellular signaling molecules that activate the toll-like receptor 4 (TLR-4)/nuclear factor-kappaB (NF-κB) pathway, leading to increased production of pro-inflammatory cytokines and other inflammatory mediators [18]. Evidence further suggests that BPA may directly stimulate the TLR-4/myeloid differentiation factor 2 (MD2) receptor complex, thereby reinforce NF-κB activation and sustain the inflammatory response [19]. Persistent activation of this signaling cascade promotes inflammatory cell recruitment, cardiomyocyte apoptosis, and adverse myocardial remodeling, ultimately exacerbating cardiac dysfunction [20]. The cellular response to oxidative stress is largely coordinated by the sirtuin 1 (SIRT1)/nuclear factor erythroid 2-related factor 2 (Nrf2) signaling, a master regulator of endogenous antioxidant defenses. Activation of the SIRT1/Nrf2 axis preserves myocardial redox homeostasis, maintains mitochondrial function, and suppresses inflammatory signaling, whereas disruption of this pathway has been implicated in the pathogenesis of oxidative stress-related cardiovascular diseases [21,22]. Mechanistically, SIRT1 has been implicated in the regulation of the Nrf2/ARE antioxidant pathway, promoting the expression of cytoprotective and phase II detoxifying enzymes, including heme oxygenase-1 (HO-1), while simultaneously suppressing inflammatory signaling through deacetylation of NF-κB [23,24]. Moreover, SIRT1 modulates the activity of hypoxia-inducible factor-1α (HIF-1α), an adaptive transcription factor that, together with TXNRD1, plays a critical role in maintaining mitochondrial integrity, facilitating cellular adaptation to oxidative stress, and protecting cardiomyocytes against oxidative and inflammatory injury [25,26,27,28]. Therefore, pharmacological interventions capable of restoring the SIRT1/Nrf2/HO-1 axis while preserving HIF-1α- and TXNRD1-mediated cytoprotective responses and suppressing TLR-4/NF-κB signaling may represent a promising strategy for mitigating BPA-induced cardiac injury.

Nifuroxazide (NFZ) is an oral nitrofuran derivative that has been employed as an intestinal antiseptic and antidiarrheal agent [29]. However, recent pharmacological investigations have unveiled its pleiotropic properties, extending beyond its traditional use [29]. NFZ is recognized as a potent inhibitor of the JAK2/STAT3 pathway, a crucial signaling cascade involved in inflammation, cell proliferation, and survival [29]. Beyond its STAT3 inhibitory activity, accumulating evidence highlights the significant antioxidant and anti-inflammatory capabilities of NFZ in various models of organ injury, including nephrotoxicity, hepatotoxicity, and pulmonary fibrosis [29,30]. Given its ability to suppress inflammation and oxidative injury through modulation of key signaling pathways, NFZ possesses remarkable potential to mitigate BPA-cardiotoxicity. While NFZ has demonstrated a wide range of pharmacological and cytoprotective properties in other contexts [29,30], its specific potential to mitigate BPA-induced cardiotoxicity has not been thoroughly explored. The novelty of the present study does not lie in the previously described antioxidant or anti-inflammatory properties of NFZ, but in examining these properties in the context of BPA-induced myocardial injury and characterizing their association with the TLR-4/NF-κB and SIRT1/Nrf2/HO-1 signaling. Accordingly, the present study investigated the effects of NFZ in a rat model of BPA-induced cardiotoxicity, with emphasis on its modulation of redox balance, and the TLR-4/NF-κB and SIRT1/Nrf2/HO-1 signaling pathways.

2. Materials and Methods

2.1 Animals and Experimental Design

Twenty-four 9–10-week-old adult male Wistar rats (190–220 g, VACSERA, Giza, Egypt) were obtained and housed under controlled environmental conditions on a 12-h light/dark cycle with *ad libitum* access to food and water. After one week of acclimatization, the rats were randomly assigned to four groups (n = 6) using a random-number table. All 24 animals completed the study, and no animals or experimental units were excluded from the subsequent analyses (n = 6 per group). The sample size (n = 6 animals per group) was determined based on previously published studies using similar experimental models and assessing comparable biochemical, histological and molecular endpoints. This is a widely established experimental model, and the selected group size was consistent with those used in comparable studies. The control group received corn oil together with 0.5% carboxymethylcellulose (CMC) vehicles by oral gavage, and the NFZ group received 50 mg/kg/day NFZ [31] (Hikma Pharmaceuticals, Giza, Egypt) suspended in 0.5% CMC (Sigma, St. Louis, MO, USA) and corn oil by

oral gavage. The BPA group received 25 mg/kg/day BPA (Lanxess, Cologne, Germany) [32] dissolved in corn oil and 0.5% CMC by oral gavage. The BPA + NFZ group received both BPA in corn oil and NFZ in 0.5% CMC concurrently by oral gavage. All treatments were administered once daily for 28 consecutive days. The BPA dose was selected to establish a reproducible repeated-exposure model of BPA-induced tissue injury [32].

2.2 Sample Collection and Preparation

Twenty-four hours after the final dose, rats were anesthetized with an intraperitoneal injection of 80 mg/kg ketamine (Sigma-Tec, Giza, Egypt) and 10 mg/kg xylazine (ADWIA, Cairo, Egypt). Ketamine/xylazine mixture was prepared by mixing ketamine (100 mg/mL), xylazine (20 mg/mL), and normal saline at a ratio of 4:2.5:3.5 (*v*/*v*/*v*). The mixture was administered at 0.2 mL/100 g body weight. Blood was collected and serum was separated by centrifugation (805 ×g for 15 min at 4 °C) and stored at –20 °C for biochemical analysis. Following blood collection, the animals were euthanized by cervical dislocation. The hearts were quickly excised, rinsed in ice-cold PBS, and the left ventricle tissue was divided into portions. One portion was fixed in 10% neutral buffered formalin for histopathological and immunohistochemical (IHC) investigations, another was homogenized in chilled 10 mM Tris-HCl buffer (pH 7.4), and the remaining tissue was immediately snap-frozen in liquid nitrogen and preserved at –80 °C.

2.3 Assessment of Cardiac Injury Biomarkers, Oxidative Stress and Inflammation

Serum creatine kinase MB (CK-MB) and lactate dehydrogenase (LDH) were measured using Spinreact kits (Girona, Spain; Cat. no. 41220 and 1001054, respectively). Cardiac troponin I (cTnI) in serum and tumor necrosis factor (TNF)-α and interleukin (IL)-1β in the heart homogenates were quantified using ELISA kit (Elabscience, Wuhan, China; Cat. no.: E-EL-R1253, E-EL-R2856, and E-EL-R0012, respectively). Myocardial tissue homogenates were used to determine malondialdehyde (MDA), reduced glutathione (GSH), superoxide dismutase (SOD) and catalase using colorimetric kits (BioDiagnostic, Cairo, Egypt; Cat. no.: MD2528, TA2511, SD2521, and CA2517, respectively). HO-1 activity was determined spectrophotometrically according to a previously established protocol [33].

2.4 Histopathological and IHC Analysis

Fixed cardiac tissues were dehydrated through a graded ethanol series, cleared in xylene, and embedded in paraffin wax. Sections (5 µm thickness) were cut and stained with hematoxylin and eosin (H&E), Masson's trichrome (MT), Sirius red (SR), or Periodic acid-Schiff (PAS). Histological damage was evaluated blindly by a histopathologist using a scoring system (0 to 4) based on the extent of cellular degeneration, vascular congestion, cardiomyocyte hypotrophy, and pyknosis. The cross-sectional diameter of cardiomyocytes and corresponding nuclear diameter were measured using ImageJ (NIH, Bethesda, MD, USA). SR-stained areas were quantified using ImageJ (NIH, USA). For IHC analysis, tissue sections were deparaffinized, rehydrated, and subjected to heat-induced antigen retrieval in citrate buffer (0.05 M, pH 6.8). Endogenous peroxidase activity was blocked with 3% hydrogen peroxide, followed by blocking of non-specific protein binding sites with normal goat serum. Sections were incubated overnight at 4 °C with primary antibodies against TLR-4, NF-κB p65, SIRT1, Nrf2, and HIF-1α (Biospes, Chongqing, China; Cat. no.: YPA2203, YPA2934, YPA2140, YPA1621, and YPA2332, respectively) diluted 1:100, and TXNRD1 antibody (Abcam, Waltham, MA, USA; Cat. no. ab124954) diluted 1:1000. After incubation with appropriate HRP-conjugated secondary antibody (Invitrogen, Waltham, MA, USA; Cat. no.: 31460) diluted 1:1000, immunoreactivity was visualized using 3,3′-diaminobenzidine (DAB), and nuclei were counterstained with hematoxylin. Representative images were acquired using a light microscope, and immunostaining intensity was quantified with ImageJ (NIH, USA) from six randomly selected microscopic fields per animal. Before quantitative image analysis, all images were assigned anonymized codes, and treatment identities were concealed. Quantitative measurements were subsequently performed by an investigator blinded to treatment allocation and sample identity.

2.5 Quantitative Reverse Transcription Polymerase Chain Reaction (qRT-PCR)

Total RNA was isolated from frozen cardiac tissue using TRIzol (Invitrogen, USA) according to the manufacturer's recommendations. RNA concentration and purity were assessed spectrophotometrically by measuring the A260/A280 ratio. cDNA was synthesized from 1 µg of total RNA using a high-capacity reverse transcription kit (ThermoFisher, Waltham, MA, USA; Cat. no. 4374967). qRT-PCR was subsequently performed using SYBR Green Master Mix (Qiagen, Germantown, MD, USA; Cat. no. 204143) and gene-specific primers for *Sirt1*, *Nrf2*, *Hif1a*, and *Txnrd1*, with *Actb* serving as the internal reference gene (**Supplementary Table 1**). Relative mRNA expression levels were calculated using the $2^{-\Delta\Delta Ct}$ method [34].

2.6 Molecular Docking

Molecular docking was performed to investigate the potential interactions of BPA with SIRT1 (PDB ID: 5BTR), HO-1 (PDB ID: 1DVE), and TXNRD1 (PDB ID: 4KPR). Prior to docking, the selected protein structures were processed in AutoDockTools (v1.5.6). Protein preparation involved deletion of water molecules, incorporation of polar hydrogen atoms, and assignment of the appropriate atomic

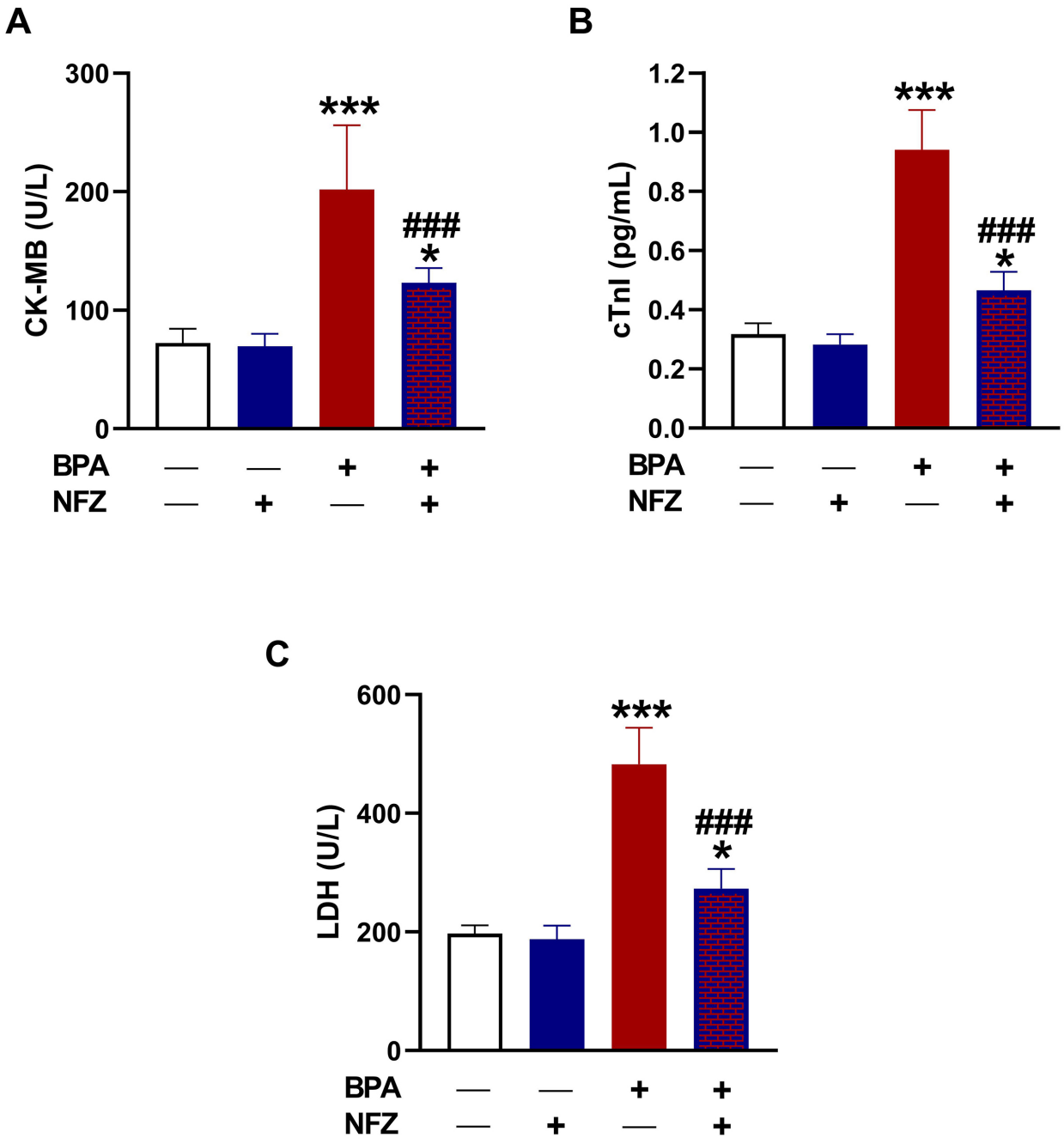


Fig. 1. NFZ reduces circulating CK-MB (A), cTnI (B), and LDH (C) in BPA-administered rats. Data are mean ± SD, (n = 6). $^{*}p < 0.05$ and $^{***}p < 0.001$ versus Control. $^{###}p < 0.001$ versus BPA. NFZ, nifuroxazide; cTnI, cardiac troponin I; CK-MB, creatine kinase MB; LDH, lactate dehydrogenase; BPA, bisphenol A.

charges. The ligands were subjected to energy minimization before being used for docking calculations. Docking was performed using AutoDock Vina implemented in PyRx (v0.8) [35]. EX-527, heme, and TRi-1 were used as reference ligands for SIRT1, HO-1, and TXNRD1, respectively. The resulting docking poses and protein–ligand interactions were analyzed and visualized using PyMOL (v2.3.2) and LigPlot+ (v2.2.8) [36].

2.7 Statistical Analysis

All data are presented as mean ± standard deviation (SD). Data normality was evaluated using the Shapiro-Wilk test. Statistical analyses were performed using GraphPad Prism version 8.0 (GraphPad, San Diego, CA, USA). Differences among experimental groups were analyzed by one-way ANOVA followed by Tukey's multiple-comparison test for post-hoc analysis. Statistical significance was set

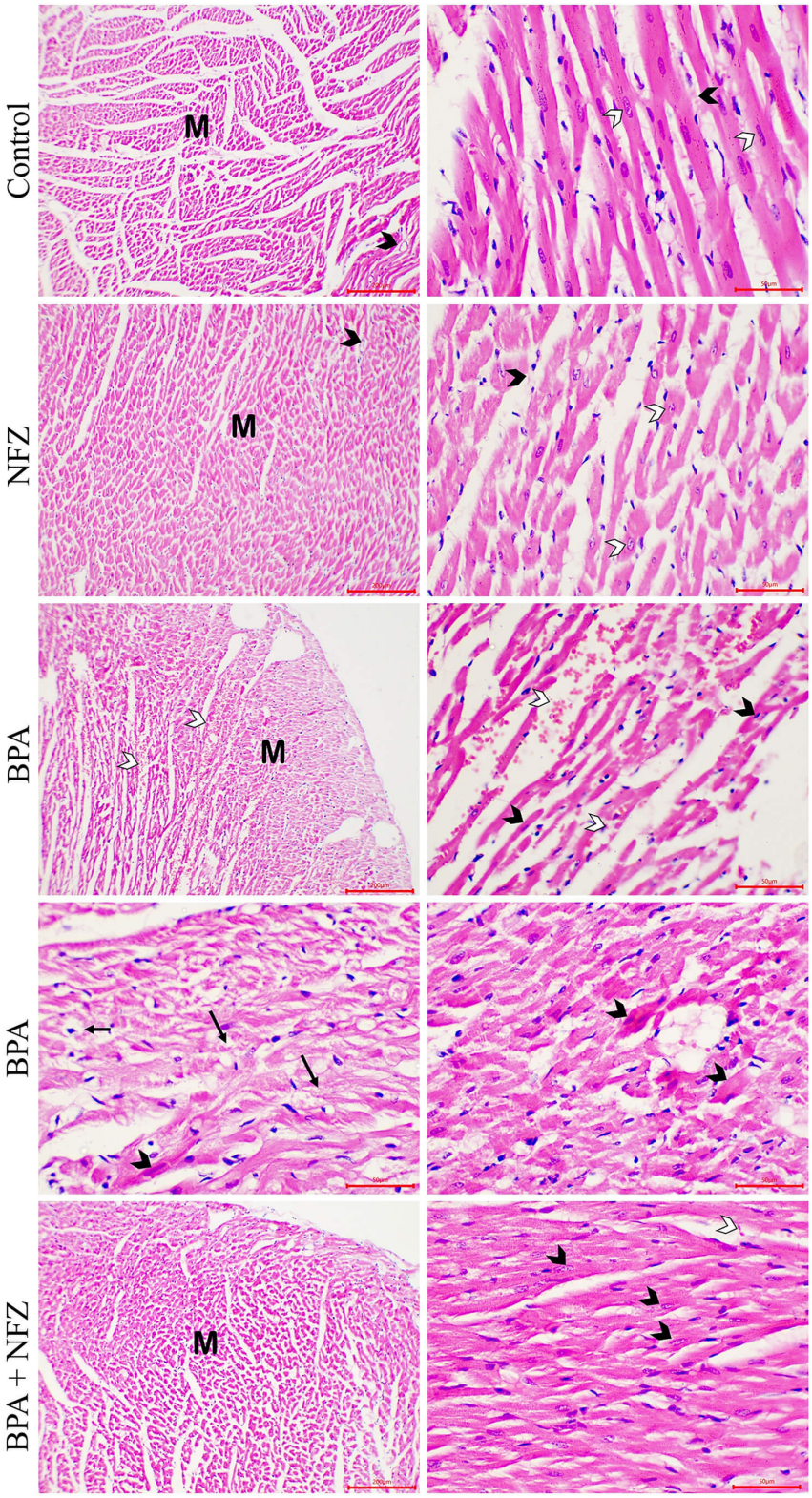


Fig. 2. NFZ ameliorates cardiac histopathological alterations induced by BPA. H&E-stained heart sections of the control and NFZ-treated rats showing normal cardiac muscle fibers (M) with oval central nuclei (white arrowheads), and normal blood vessels (black arrowheads); BPA-administered group revealing dilated congested blood vessels (white arrowheads), vacuolated cardiac muscle fibers (black arrowheads), myocyte hypotrophy, pyknosis, and hypereosinophilia (black arrows); and BPA-administered rats cotreated with NFZ showing restoration of the histological structure of the cardiac muscle fibers (M and black arrowheads) and the blood vessels (white arrowhead). (Scale bar = 200 µm (left panel) and 50 µm (right panel)). H&E, hematoxylin and eosin.

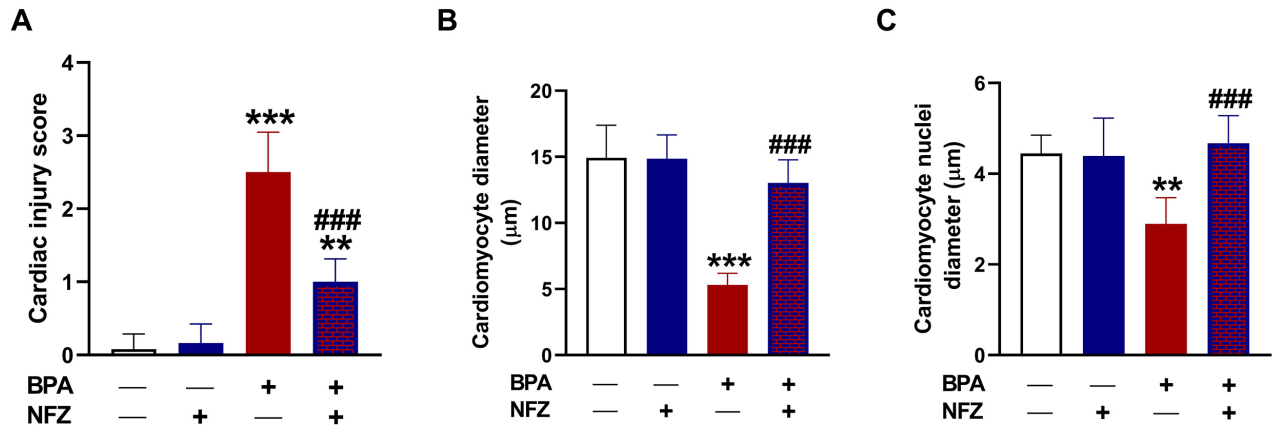


Fig. 3. NFZ mitigates BPA-induced heart tissue injury (A) and attenuated BPA-induced reduction in the diameter of cardiomyocytes (B) and their nuclei (C). Data are mean ± SD, ($n = 6$). $^{**}p < 0.01$ and $^{***}p < 0.001$ versus Control. $^{###}p < 0.001$ versus BPA. SD, standard deviation.

at $p < 0.05$. For descriptive visualization, group means for each parameter were standardized across the four experimental groups using parameter-wise Z scores. The resulting heatmap was used to display treatment-related patterns across parameters with different measurement units.

3. Results

3.1 NFZ Protects Against BPA-Induced Myocardial Injury

The cardioprotective potential of NFZ was initially assessed by measuring serum biomarkers indicative of myocardial damage (Fig. 1A–C). Rats exposed to BPA exhibited pronounced elevations in circulating CK-MB, cTnI, and LDH compared with the control group ($p < 0.001$), confirming significant cardiac injury. NFZ markedly reduced these biomarkers ($p < 0.001$ versus BPA), whereas treatment with NFZ alone produced no detectable changes relative to control animals.

Microscopic examination of myocardial sections corroborated the biochemical findings (Fig. 2). Hearts from the control and NFZ groups displayed preserved myocardial architecture with orderly arranged cardiac fibers, centrally positioned nuclei, and normal interstitial spaces. In contrast, BPA administration produced structural abnormalities, including vascular congestion, cytoplasmic vacuolation, cardiomyocyte atrophy, and intensely eosinophilic fibers containing pyknotic nuclei. These pathological alterations were substantially attenuated in rats receiving NFZ, which exhibited marked restoration of myocardial morphology. Morphometric analysis (Fig. 3A–C) further demonstrated that BPA significantly increased the myocardial injury score while reducing both cardiomyocyte size and nuclear diameter ($p < 0.001$). These adverse effects were significantly ameliorated by NFZ treatment. Histochemical evaluation provided additional confirmation of myocardial protection. SR and MT staining revealed pronounced collagen accumulation following BPA exposure, and PAS staining revealed an increase in PAS-positive material (Fig. 4). Image analysis revealed a significant increase in collagen staining after BPA exposure ($p < 0.001$), with significant attenuation after NFZ supplementation ($p < 0.001$; **Supplementary Fig. 1**). These abnormalities were markedly diminished in the BPA + NFZ group, while no appreciable histological differences were observed between the control and NFZ-treated animals.

3.2 NFZ Alleviates Oxidative Stress Induced by BPA

Exposure to BPA disturbed myocardial redox homeostasis, as reflected by a significant elevation in MDA levels together with marked reductions in GSH, SOD, and catalase (Fig. 5A–D; $p < 0.001$). Co-administration of NFZ effectively counteracted these alterations by lowering MDA and restoring antioxidants ($p < 0.001$). NFZ alone had no significant effect on any of the evaluated oxidative stress parameters.

3.3 NFZ Suppresses Myocardial Inflammatory Signaling Triggered by BPA

IHC demonstrated minimal basal expression of TLR-4 and NF-κB p65 in myocardial sections obtained from control and NFZ-treated rats (Fig. 6A–C). BPA exposure markedly enhanced the immunoreactivity of both proteins ($p < 0.001$). NFZ significantly attenuated the expression of TLR-4 and NF-κB p65 compared with BPA-treated animals ($p < 0.001$). Likewise, BPA markedly increased myocardial TNF-α and IL-1β (Fig. 6D,E), whereas these inflammatory cytokines were significantly reduced by NFZ co-treatment. Basal inflammatory marker expression remained unchanged in rats receiving NFZ alone.

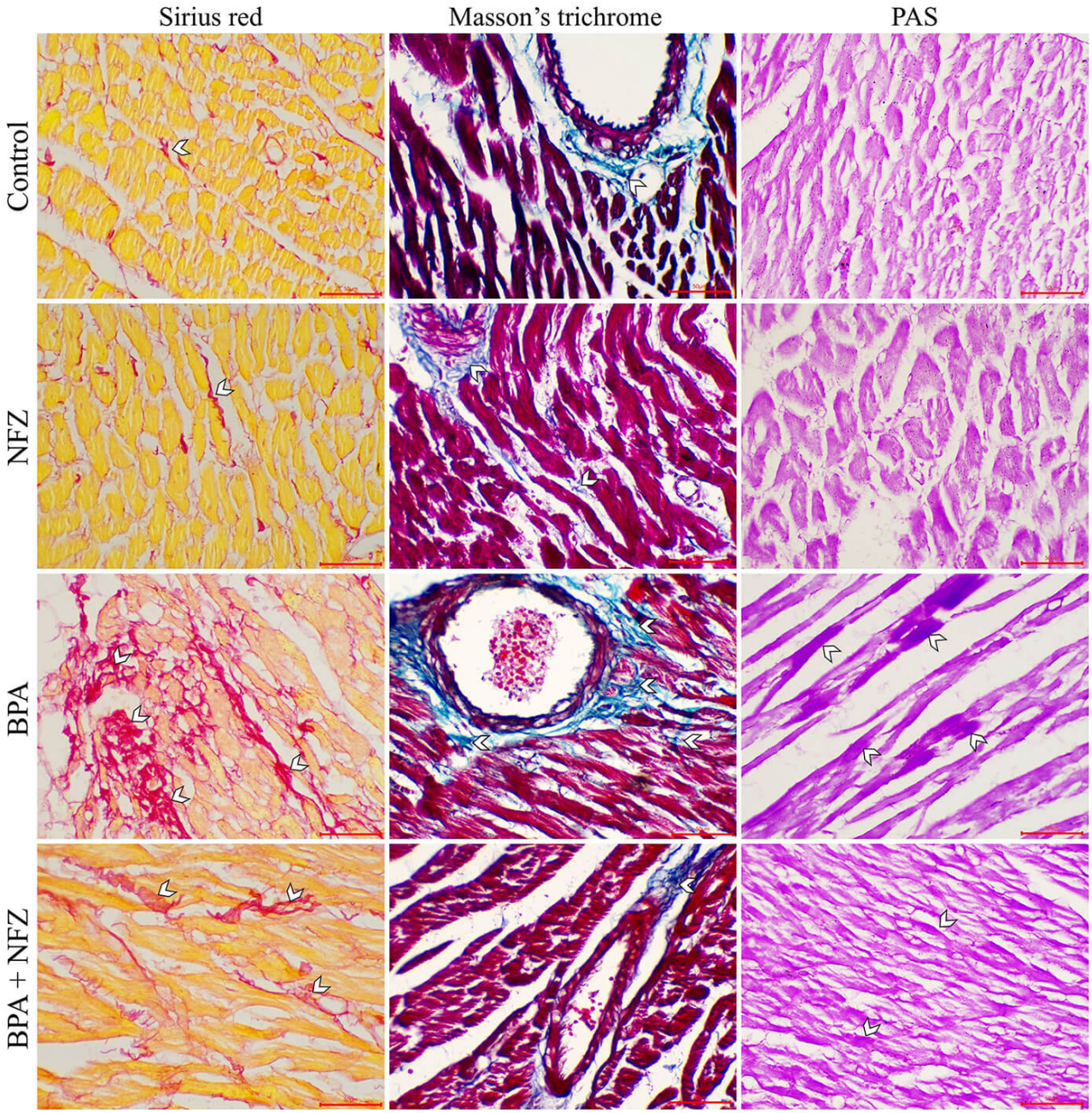


Fig. 4. Photomicrographs of Sirius red-, Masson's trichrome-, and PAS-stained heart sections. Sirius red and Masson's trichrome staining shows little collagen between the muscle fibers (white arrowheads) in control and NFZ-supplemented rats, increased collagen in BPA-administered rats and normal collagen fibers in BPA-administered rats co-treated with NFZ (white arrowheads). PAS staining shows normal distribution and affinity in control and NFZ-supplemented rats, whereas BPA-administered rats show an increase in the PAS intensity (white arrowheads). Co-treatment with NFZ decreased PAS staining in BPA-administered rats. (Scale bar = 50 µm). PAS, Periodic acid-Schiff.

3.4 NFZ Preserves the Myocardial SIRT1/Nrf2/HO-1 Antioxidant Pathway

Analysis of gene expression revealed that BPA significantly suppressed myocardial SIRT1 and Nrf2 transcripts relative to the control group (Fig. 7A,B; $p < 0.001$). Concurrent administration of NFZ largely prevented these reductions. IHC assessment produced similar findings, with BPA markedly decreasing SIRT1 and Nrf2, while NFZ significantly enhanced the immunostaining intensity of both proteins (Fig. 7C–E; $p < 0.001$). Furthermore, BPA reduced HO-1 enzymatic activity (Fig. 7F), whereas NFZ effectively restored it.

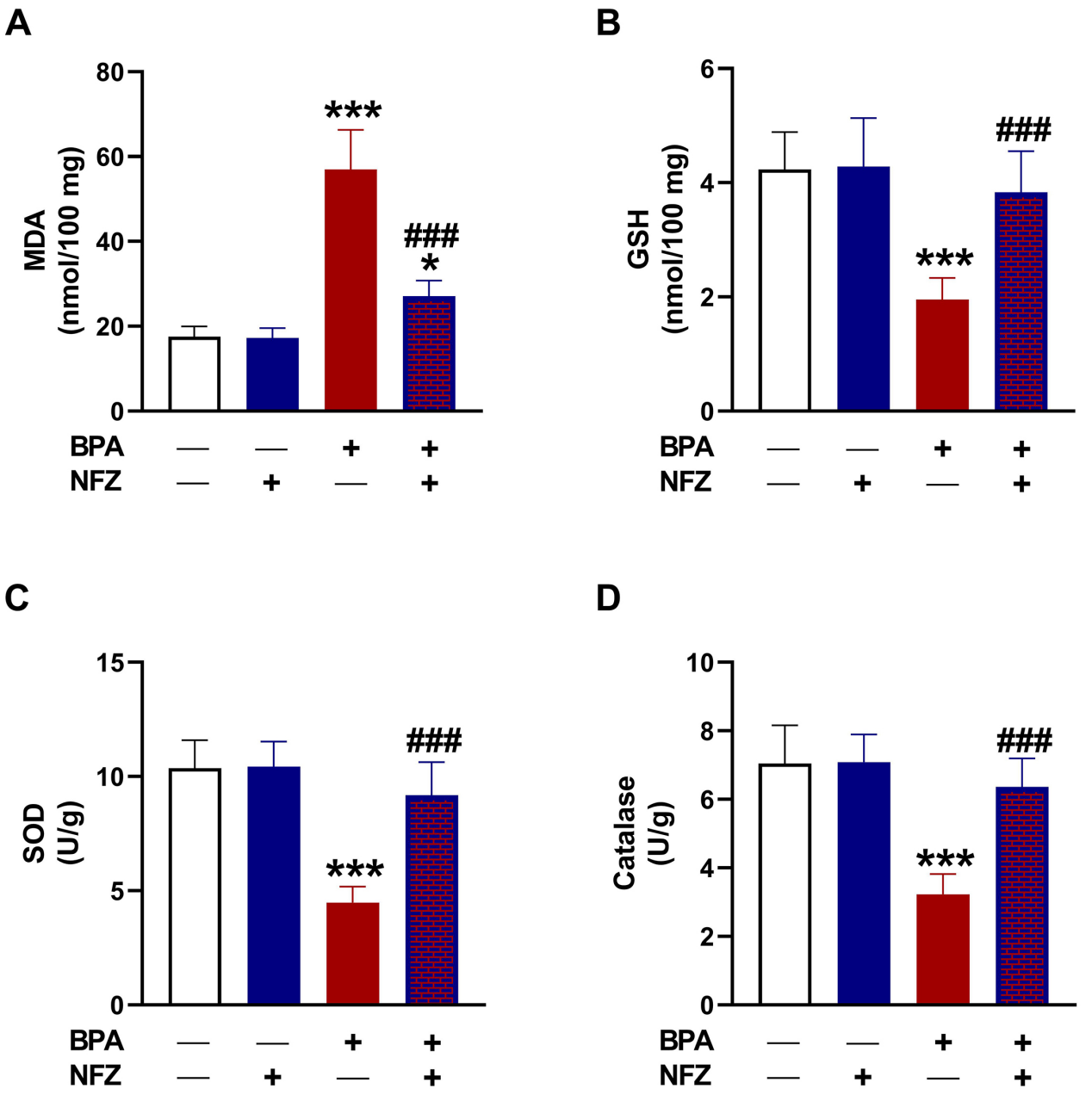


Fig. 5. NFZ attenuates cardiac oxidative stress in BPA-administered rats. NFZ ameliorated MDA (A), GSH (B), SOD (C), and catalase (D). Data are mean ± SD, ($n = 6$). $^{*}p < 0.05$ and $^{***}p < 0.001$ versus Control. $^{###}p < 0.001$ versus BPA. MDA, malondialdehyde; GSH, reduced glutathione; SOD, superoxide dismutase; BPA, bisphenol A.

3.5 NFZ Reverses BPA-Induced Suppression of HIF-1α and TXNRD1

BPA significantly downregulated the mRNA of both HIF-1α and TXNRD1 compared with controls (Fig. 8A,B; $p < 0.001$). These transcriptional changes were accompanied by markedly reduced HIF-1α and TXNRD1 immunoreactivity (Fig. 8C–E). NFZ significantly restored both gene and protein expression relative to BPA-exposed rats ($p < 0.001$), while no significant differences were detected between the control and NFZ-alone groups.

3.6 Molecular Docking Analysis Reveals Potential Interactions of BPA With SIRT1, HO-1, and TXNRD1

Molecular docking was performed to investigate the potential interactions of BPA with SIRT1, HO-1, and TXNRD1 (Figs. 9,10,11). BPA showed predicted binding energies of –6.9 kcal/mol with SIRT1, –7.3 kcal/mol with HO-1, and –7.3 kcal/mol with TXNRD1. For SIRT1, BPA exhibited a binding mode that partially overlapped with that of the reference inhibitor EX-527, which showed a lower predicted binding energy of –7.7 kcal/mol. Several residues, including Asp292, Ala295, Asp298, Gln294, and

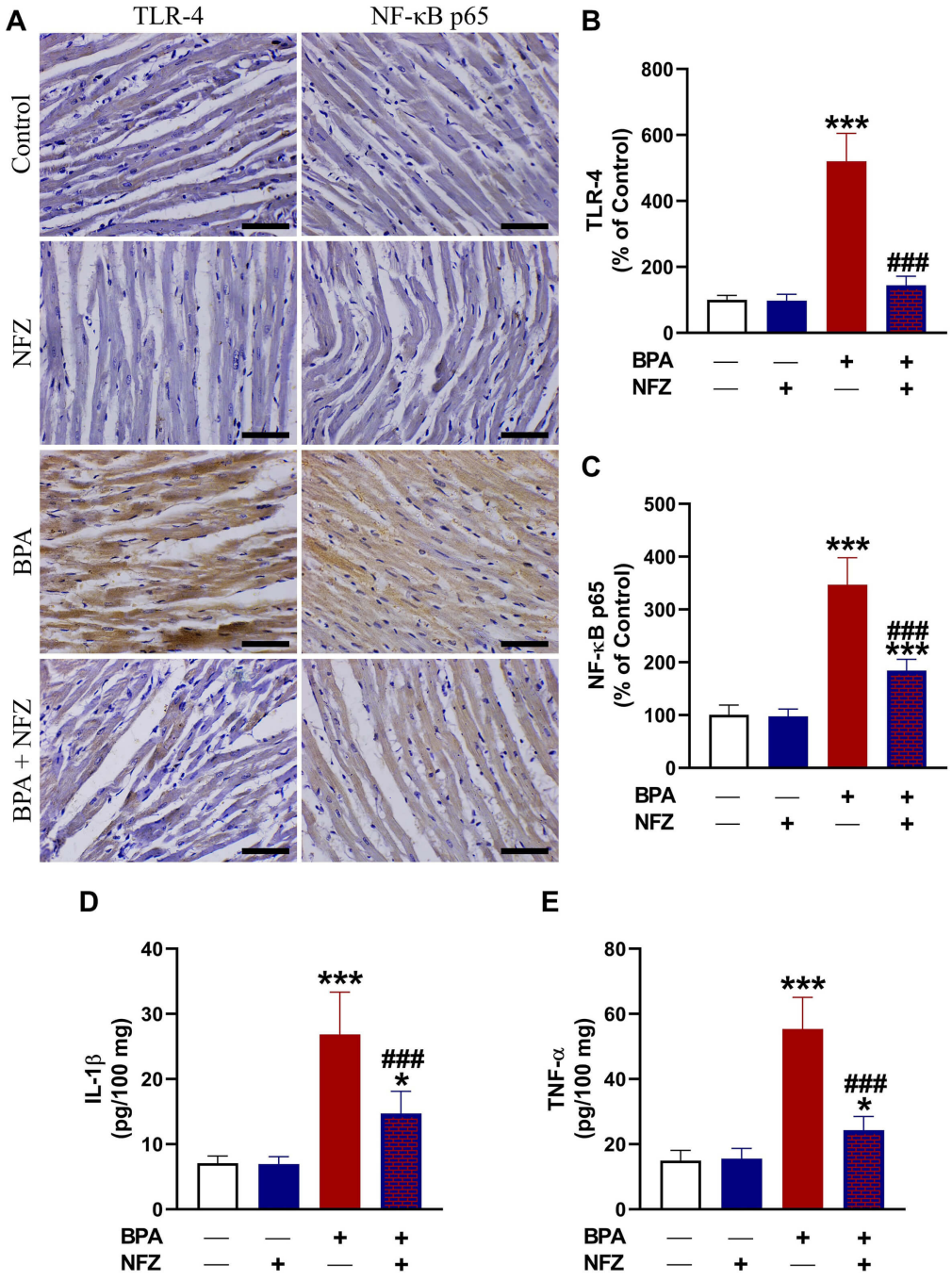


Fig. 6. NFZ attenuates TLR-4/NF-κB signaling in the heart of BPA-administered rats. (A) Representative IHC photomicrographs showing TLR-4 and NF-κB p65. BPA increased immunoreactivity, whereas NFZ co-administration suppressed these changes. Scale bar = 50 µm. (B,C) Quantitative analysis of TLR-4 (B) and NF-κB p65 (C) immunostaining expressed as a percentage of the control group. (D,E) NFZ ameliorates cardiac IL-1β (D) and TNF-α (E) in BPA-administered rats. Data are mean ± SD, (n = 6). $^{*}p < 0.05$ and $^{***}p < 0.001$ versus Control. $^{###}p < 0.001$ versus BPA. TLR-4, toll-like receptor 4; NF-κB, nuclear factor-kappaB; IHC, immunohistochemical; IL, interleukin; TNF, tumor necrosis factor.

Pro212, were common to the predicted interaction profiles of BPA and EX-527 (Fig. 9). For HO-1, BPA displayed a predicted binding energy of –7.3 kcal/mol and showed overlapping interactions with heme involving Met34, Gly139, Thr135, Phe207, Asn210, and Phe214 (Fig. 10). For TXNRD1, BPA showed a predicted binding energy of –7.3 kcal/mol, compared with –7.6 kcal/mol for the reference inhibitor TRi-1. The two ligands shared interaction with Leu75 (Fig. 11).

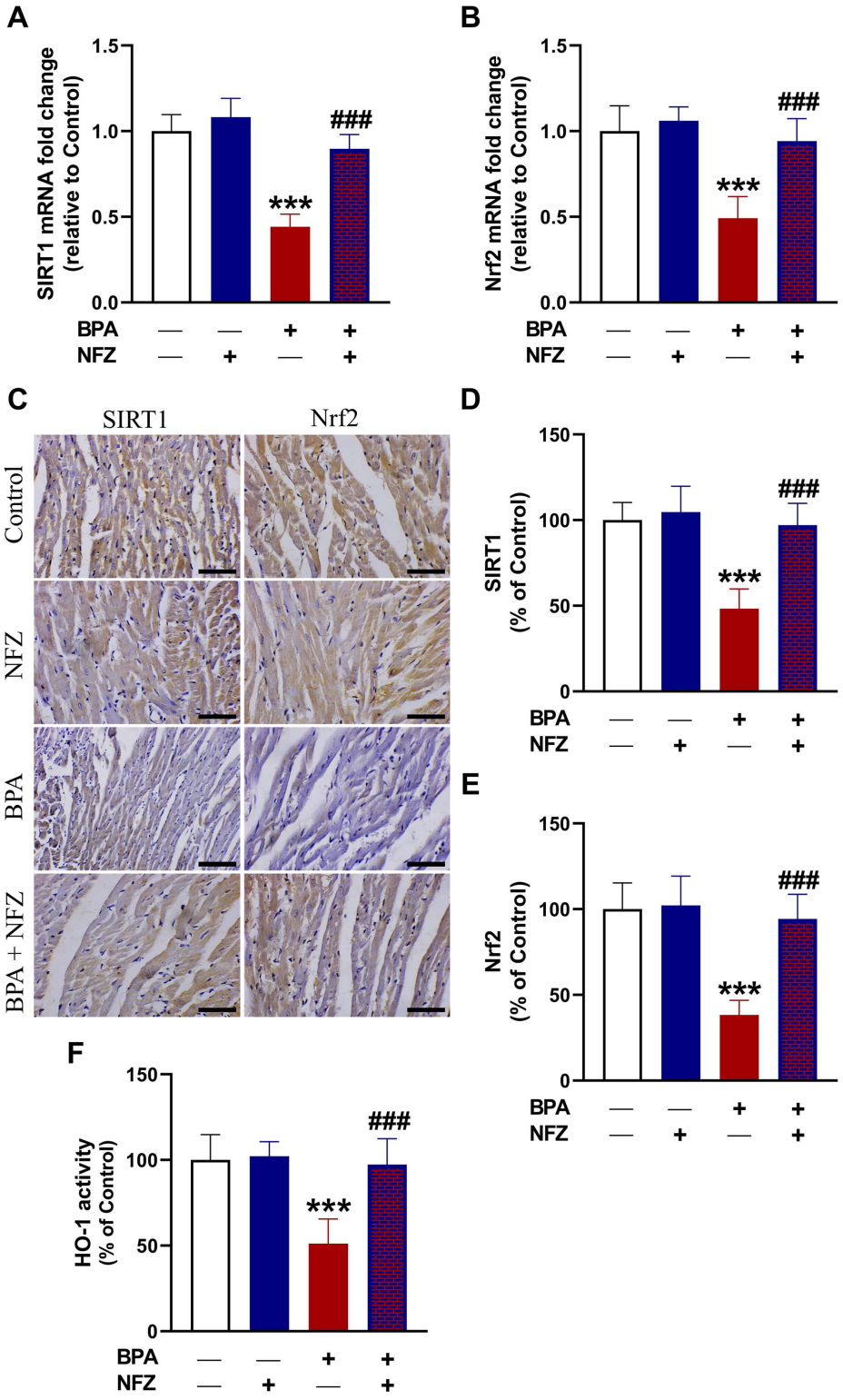


Fig. 7. NFZ enhances cardiac SIRT1/Nrf2/HO-1 pathway in BPA-administered rats. (A,B) BPA downregulated SIRT1 and Nrf2 mRNA, changes that were significantly attenuated by NFZ. (C) Representative images showing cardiac SIRT1 and Nrf2 immunostaining. Scale bar = 50 µm. (D,E) Quantitative analysis of SIRT1 and Nrf2 immunostaining expressed as a percentage of the control group showing suppressed expression in BPA-administered rats and alleviation in NFZ co-treated rats. (F) NFZ increased cardiac HO-1 activity in BPA-administered rats. Data are mean ± SD, (n = 6). $^{***}p < 0.001$ versus Control. $^{###}p < 0.001$ versus BPA. SIRT1, sirtuin 1; Nrf2, nuclear factor erythroid 2-related factor 2; HO-1, heme oxygenase-1.

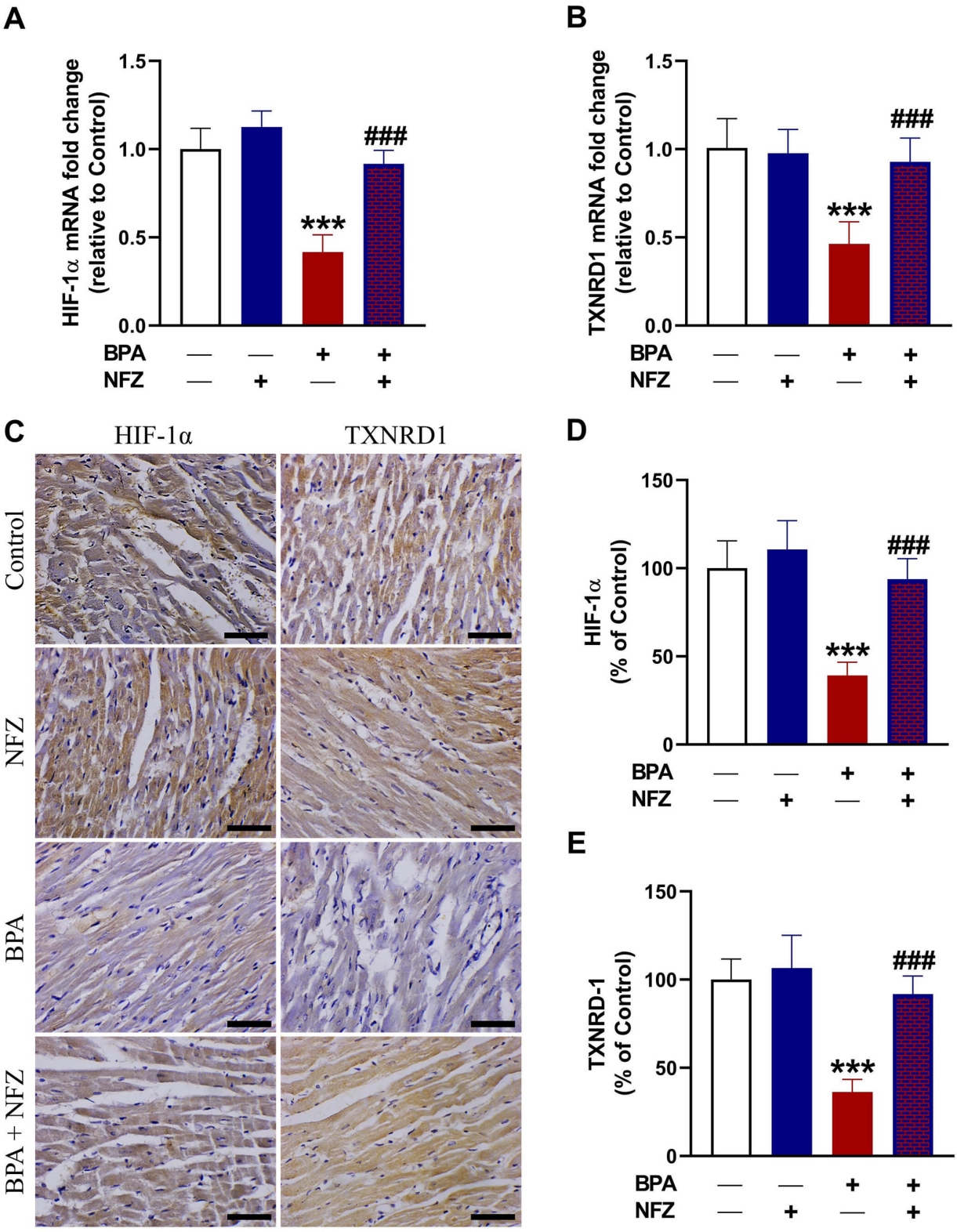


Fig. 8. NFZ alleviates cardiac HIF-1α and TXNRD1 in BPA-administered rats. (A,B) NFZ enhanced HIF-1α (A) and TXNRD1 (B) mRNA in BPA-administered rats. (C) Representative images showing cardiac HIF-1α and TXNRD1 immunostaining. Scale bar = 50 μm. (D,E) NFZ enhanced cardiac HIF-1α and TXNRD1 expression in BPA-administered rats. Data are mean ± SD, (n = 6). $^{***}p < 0.001$ versus Control and $^{###}p < 0.001$ versus BPA. HIF-1α, hypoxia-inducible factor-1α; TXNRD1, thioredoxin reductase 1.

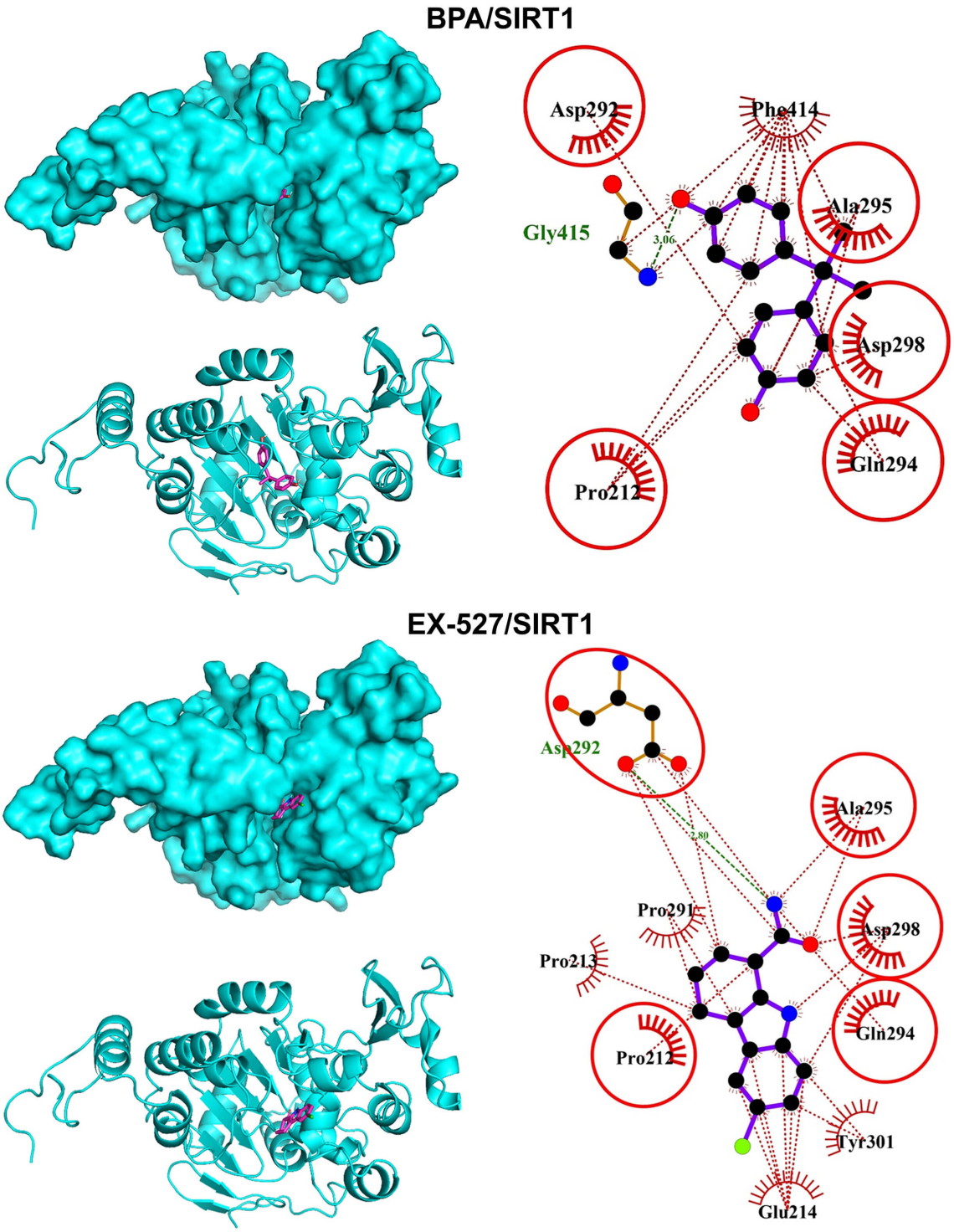


Fig. 9. Molecular docking of BPA and EX-527 with SIRT1. BPA showed a predicted binding energy of –6.9 kcal/mol, compared with –7.7 kcal/mol for EX-527. Circled residues indicate amino acids involved in interactions with both ligands.

3.7 Effects of BPA and NFZ on Body Weight

Body weight was monitored throughout the 28-day experimental period (**Supplementary Fig. 2**). Control and NFZ-treated rats exhibited progressive increases in body weight, 12.80% and 15.51%, respectively. In contrast, BPA-treated rats showed a 10.49% body weight loss over the experimental period. Concomitant NFZ treatment attenuated this reduction, with the BPA + NFZ group exhibiting an 8.76% body weight gain.

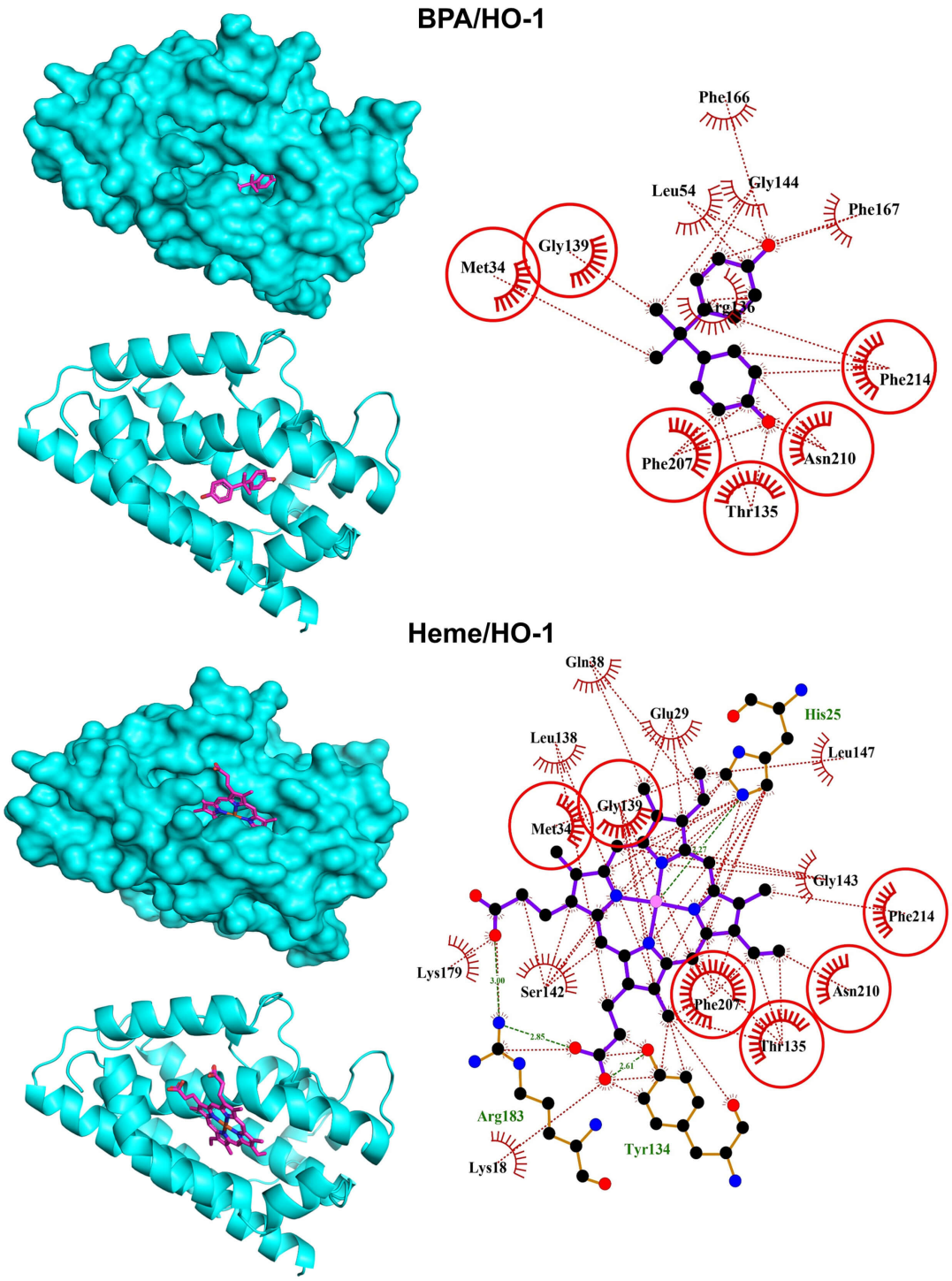


Fig. 10. Molecular docking of BPA and heme with HO-1. BPA showed a predicted binding energy of –7.3 kcal/mol. Circled residues indicate amino acids shared between the BPA- and heme-binding interaction profiles.

3.8 Standardized Group-Level Patterns of BPA-Induced Cardiotoxicity and NFZ Protection

A standardized heatmap was used to visualize treatment-related changes across cardiac injury, oxidative, and inflammatory parameters (Fig. 12). BPA produced a distinct adverse profile characterized by increased cTnI, CK-MB, LDH, tissue injury score, collagen, MDA, TLR-4, NF-κB p65, IL-1β, and TNF-α, together with reduced GSH, SOD, catalase, SIRT1, Nrf2, HO-1, HIF-1α, and TXNRD1. The BPA + NFZ group generally showed a shift toward the control profile, with lower standardized values for injury, oxidative, and inflammatory parameters and higher stan-

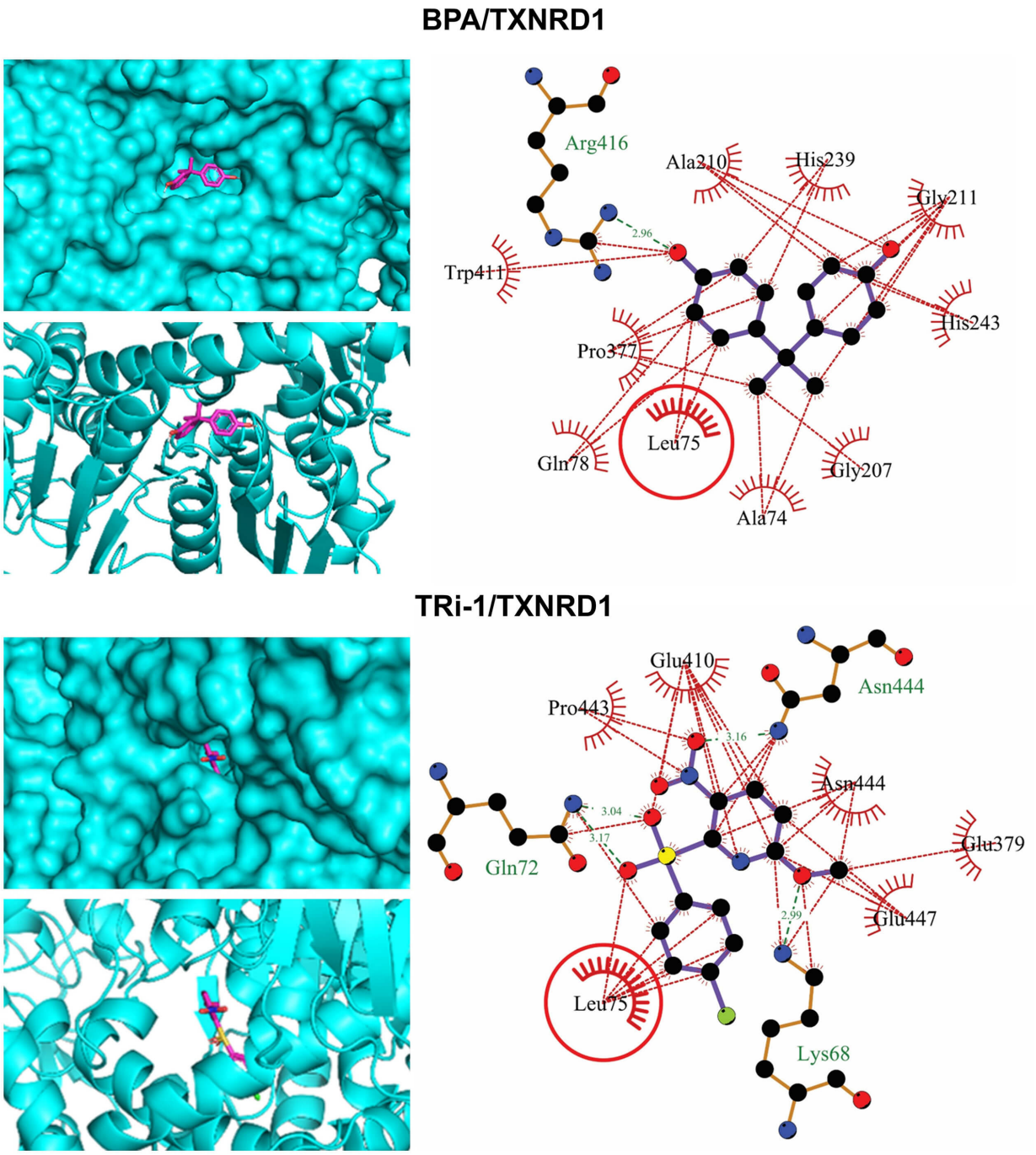


Fig. 11. Molecular docking of BPA and TRi-1 with TXNRD1. BPA and TRi-1 showed predicted binding energies of –7.3 and –7.6 kcal/mol, respectively. The circled residue indicates the amino acid shared by the two interaction profiles.

dardized values for antioxidant-related parameters. NFZ alone remained broadly similar to the control group (Fig. 12).

4. Discussion

The escalating prevalence of cardiovascular diseases has been increasingly linked to environmental pollutants, with BPA standing out as a prominent EDC with established cardiotoxic potential [10,11]. Human exposure to BPA is virtually unavoidable due to its widespread presence in numerous industrial and consumer products. The cardiotoxic effects of BPA necessitate the exploration of pharmacological agents capable of mitigating its deleterious effects on the heart. NFZ has recently attracted attention for its diverse pharmacological profile, including antioxidant and anti-inflammatory properties [30,37]. This study represents the first evaluation of NFZ's efficacy against BPA-induced cardiotoxicity, focusing on its ability to preserve structural

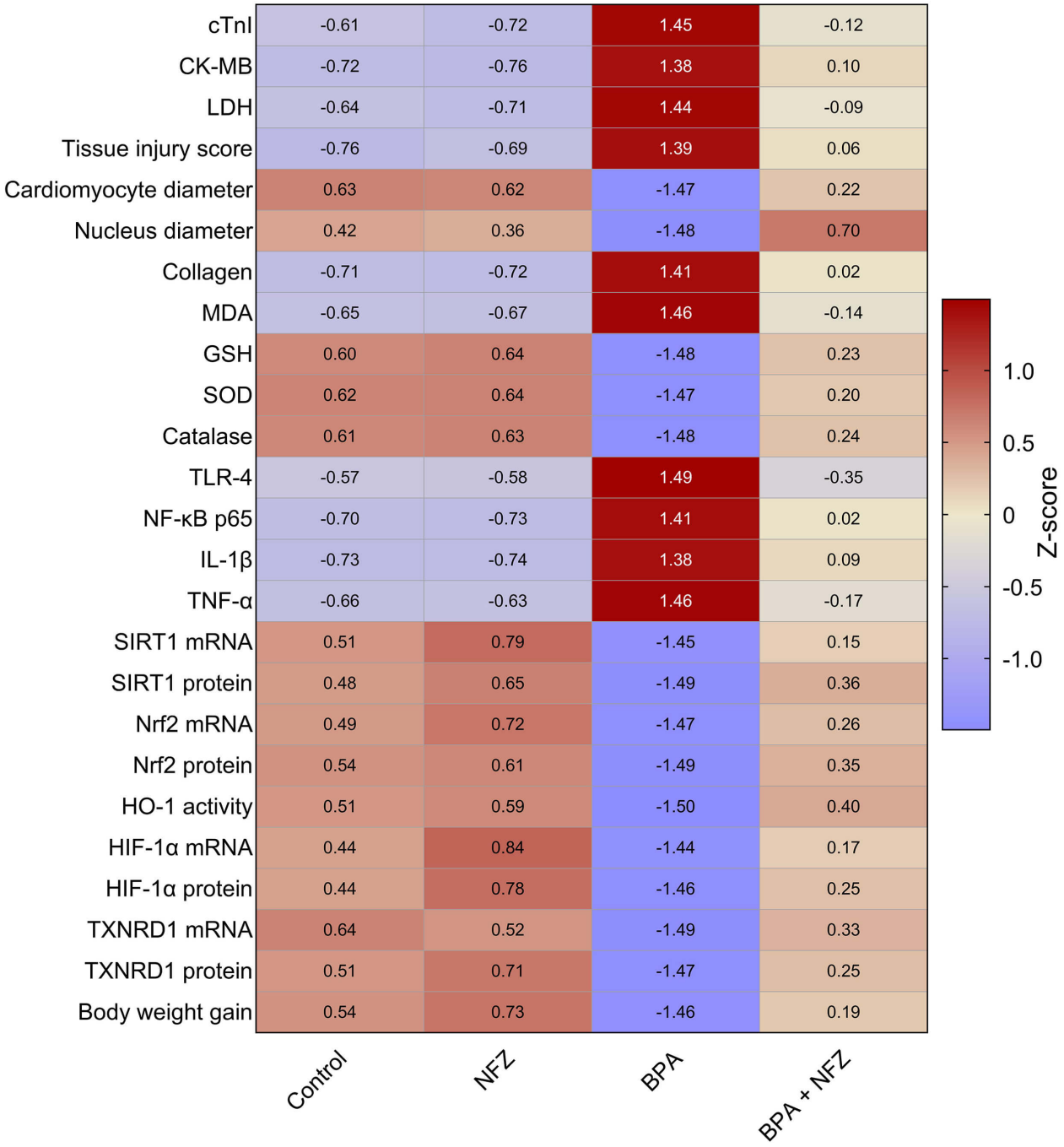


Fig. 12. Descriptive heatmap of standardized group-level changes in the BPA-induced cardiotoxicity model.

integrity, restore redox homeostasis, and modulate TLR-4/NF-κB and SIRT1/Nrf2/HO-1 signaling.

Our findings demonstrate that BPA exposure induces myocardial injury, as evidenced by both histopathological and biochemical alterations in the rat heart. The observed structural damage was corroborated by a significant elevation of serum cardiac biomarkers. Specifically, BPA induced marked increases in circulating LDH, cTnI, and CK-MB. cTnI is a highly specific and sensitive indicator of myocardial damage, as its release into the systemic circulation is a direct consequence of compromised cardiomyocyte membrane integrity [38]. Elevated serum CK-MB is an established biochemical indicator of myocardial injury in experimental rat models and has been associated with histological evidence of myocardial damage [39]. The elevated levels of these markers in BPA-exposed rats confirm the occurrence of myocardial injury, with the degree of leakage often correlating with the extent of histological damage. Although less specific than troponins, LDH provides additional evidence of generalized cellular injury within the heart [39,40]. Previous studies have consistently reported that BPA exposure leads to

increased blood CK-MB, serving as a reliable biochemical indicator of tissue damage [41]. The sustained elevation of these biomarkers suggests that BPA-induced injury is a progressive process that compromises the overall functional capacity of the heart, overwhelming intrinsic repair mechanisms under chronic BPA exposure. Furthermore, histopathological evaluation of BPA-treated rats revealed architectural disruption, characterized by vacuolated cardiomyocytes, dilated and congested blood vessels, myocyte hypotrophy, and hypereosinophilia with pyknotic nuclei. These findings are consistent with previous reports indicating that BPA induces degeneration and vacuolation of cardiomyocytes, leading to impaired cardiac function and remodeling [42]. Histochemical staining further demonstrated extensive extracellular matrix (ECM) remodeling in the myocardium. The marked increase in collagen deposition detected by MT and SR staining confirms the development of cardiac fibrosis, a hallmark of adverse myocardial remodeling that increases ventricular stiffness and progressively impairs cardiac function [43]. Experimental evidence suggests that BPA promotes fibrotic remodeling through activation of cardiac fibroblasts and dysregulation of collagen synthesis and ECM turnover [44]. In addition, the pronounced accumulation of PAS-positive material observed in BPA-treated hearts may indicate abnormal glycosaminoglycan and other carbohydrate-rich glycoconjugates deposition, which can disrupt myocardial architecture and valve integrity, thereby contributing to ventricular dysfunction, pathological remodeling, and the progression of cardiomyopathy. NFZ ameliorated these biochemical and histopathological abnormalities, suggesting a remarkable cardioprotective effect. The reduction in collagen deposition, as evidenced by MT and SR staining, and the decrease in PAS-positive material accumulation by NFZ, highlight its potential to prevent and reverse pathological cardiac remodeling and fibrosis induced by BPA. This cardioprotective efficacy of NFZ coincides with recent studies demonstrating its ability to attenuate cardiac injury. In this context, NFZ protected against 5-fluorouracil-induced cardiotoxicity as evidenced by ameliorated histopathological alterations and serum CK-MB, aspartate aminotransferase (AST), and LDH in rats [45], effects likely related to its antioxidant and anti-inflammatory activities [30,37].

Oxidative stress is recognized as a primary and critical driver of BPA cardiotoxicity [15,16]. BPA undergoes metabolic activation to form highly reactive intermediates that deplete cellular antioxidants and initiate LPO, leading to cellular dysfunction and death [15,16]. In our study, BPA exposure resulted in a significant elevation in myocardial MDA, a widely accepted marker of LPO, coupled with a concomitant decrease in GSH and the activities of key antioxidant enzymes, demonstrating oxidative stress. This oxidative imbalance is further intensified by BPA-induced mitochondrial injury. Mitochondria are both a primary source and a principal target of ROS; consequently, BPA-induced mitochondrial dysfunction further amplifies ROS generation, creating a self-perpetuating cycle of oxidative damage [16,46]. The present findings are consistent with previous experimental studies demonstrating that BPA disturbs cellular redox homeostasis, as evidenced by depletion of endogenous antioxidant defenses and enhanced LPO, including the kidney, testis, colon and liver [16,47,48]. Beyond causing direct oxidative damage, ROS also serve as key mediators of intracellular signaling that initiate inflammatory responses through activation of the TLR-4/NF-κB pathway, resulting in enhanced expression of pro-inflammatory mediators [18]. Moreover, BPA has been proposed to interact with the TLR-4/MD2 receptor complex, providing an additional mechanism for sustained NF-κB activation and amplification of inflammatory signaling [19]. Prolonged stimulation of this pathway perpetuates myocardial inflammation by promoting immune cell infiltration, accelerating cardiomyocyte apoptosis, and driving pathological cardiac remodeling, thereby contributing to the progressive deterioration of cardiac structure and function [20]. Previous experimental studies have demonstrated that BPA exposure activates the NF-κB signaling in several tissues, including the chicken trachea and the murine liver, colon, and kidney, thereby promoting the production of inflammatory mediators and exacerbating inflammatory responses [16,47,49].

NFZ suppressed LPO and replenished endogenous antioxidants by restoring GSH content and enhancing SOD and catalase activities. The restoration of these antioxidant defenses is crucial for neutralizing ROS and preventing further oxidative damage to myocardial tissue. The antioxidant activity of NFZ observed in the present study is consistent with previous reports demonstrating its ability to attenuate LPO in experimental models of diabetic nephropathy and methotrexate-induced intestinal injury [37,50]. Restoration of cellular redox homeostasis may also contribute to the anti-inflammatory effects of NFZ by limiting ROS-mediated activation of the TLR-4/NF-κB signaling cascade, thereby reducing the expression of downstream inflammatory mediators and interrupting the reciprocal amplification between oxidative stress and inflammation [18]. Accordingly, NFZ markedly downregulated TLR-4, NF-κB, TNF-α and IL-1β. The anti-inflammatory efficacy of NFZ may involve modulation of interconnected inflammatory signaling pathways, including STAT3 and NF-κB, which exhibit functional crosstalk in regulating inflammatory gene expression [29,51]. The present results agree with previous experimental studies reporting that NFZ effectively alleviates inflammatory responses in models of methotrexate-induced intestinal damage and BPA-associated reproductive toxicity [30,37].

The dual anti-inflammatory and antioxidant efficacy of NFZ is likely associated with upregulation of the SIRT1/Nrf2 signaling. The significant reduction in myocardial SIRT1, Nrf2, and TXNRD1 and suppressed HO-1 activity following BPA exposure suggests disruption of a

key endogenous defense mechanism that protects the heart against oxidative and inflammatory insults [21,22]. Consequently, impairment of this pathway has been closely associated with the development and progression of oxidative stress-driven cardiovascular disorders [21,22]. NFZ prevented the impact of BPA on this protective signaling in the heart of rats as shown be upregulated SIRT1, Nrf2, HO-1, and TXNRD1. As an upstream regulator of cellular stress responses, SIRT1 enhances the transcriptional activity of Nrf2, thereby promoting the expression of antioxidant and phase II detoxification enzymes, including HO-1 and TXNRD1. Nrf2 is a master transcription factor that orchestrates the expression of numerous antioxidant and phase II detoxifying enzymes [21]. HO-1 is a critical enzyme in heme catabolism that further contributes to the antioxidant defense by producing biliverdin, a potent antioxidant, and carbon monoxide, a signaling molecule with anti-inflammatory properties [52]. The reduction in TXNRD1 following BPA exposure indicates disruption of the myocardial thioredoxin antioxidant system, thereby weakening cellular redox regulation and favoring ROS accumulation, mitochondrial dysfunction, and inflammatory signaling that collectively contribute to cardiac injury [28]. Therefore, the restoration of TXNRD1 by NFZ plays a vital role in redox regulation and protection against oxidative stress.

The *in silico* analysis provides additional structural support for the potential interaction of BPA with components of this antioxidant defense network. BPA displayed favorable predicted binding energies with SIRT1, HO-1, and TXNRD1. For SIRT1, the BPA docking pose overlapped with the binding region occupied by the reference inhibitor EX-527, which showed a somewhat more favorable predicted binding energy (–7.7 kcal/mol). Several residues, including Asp292, Ala295, Asp298, Gln294, and Pro212, were common to the predicted interaction profiles of BPA and EX-527, suggesting that BPA can engage a region of SIRT1 relevant to ligand recognition. Similarly, BPA showed an overlapping interaction pattern with heme within HO-1, with Met34, Gly139, Thr135, Phe207, Asn210, and Phe214 representing common interacting residues. BPA also showed a predicted interaction with TXNRD1 that partially overlapped with the TRi-1 interaction profile, including the shared Leu75 residue; the predicted binding energy of BPA was –7.3 kcal/mol compared with –7.6 kcal/mol for TRi-1. These findings suggest that BPA has the capacity to interact with binding regions of SIRT1, HO-1, and TXNRD1 that are also recognized by their respective reference ligands. These computational predictions provide a structural rationale for further investigation of whether BPA directly interacts with or functionally affects these antioxidant proteins and may therefore complement the experimentally observed alterations in their myocardial expression. However, docking scores represent computational predictions of ligand–protein affinity and cannot by themselves establish functional inhibition, changes in enzymatic activity, or a causal relationship between BPA binding and the observed transcriptional and protein-level downregulation. Experimental studies assessing the enzymatic activities, binding kinetics, and site-specific effects of BPA on these proteins will be required to confirm this proposed mechanism.

Beyond its role in redox regulation, SIRT1 also modulates inflammatory and adaptive stress signaling through deacetylation of NF-κB and HIF-1α, highlighting its central role in preserving myocardial homeostasis under conditions of oxidative stress [25]. The upregulation of HIF-1α by NFZ provides additional layers of protection. Together with TXNRD1, HIF-1α plays a critical role in maintaining mitochondrial integrity, facilitating cellular adaptation to oxidative stress, and protecting cardiomyocytes against oxidative and inflammatory injury [26,27]. Our observations are supported by accumulating evidence identifying oxidative stress, mitochondrial dysfunction, and inflammation as interconnected mechanisms through which BPA disrupts myocardial homeostasis and promotes structural and functional cardiac abnormalities [9,10]. The ability of NFZ to modulate multiple interconnected pathways underscores its potential as a multifaceted therapeutic agent. The suppression of TLR-4/NF-κB signaling is particularly important as it directly targets the inflammatory cascade initiated by BPA, preventing the perpetuation of myocardial injury. The activation of SIRT1/Nrf2 axis, in turn, not only contributes to NF-κB deacetylation but also promotes cellular longevity and stress resistance, further enhancing cardioprotection.

The changes in body weight provide additional evidence of the effects associated with repeated BPA exposure. The marked body-weight loss in BPA-treated rats was attenuated by concomitant NFZ administration, consistent with a beneficial effect of NFZ on the overall response to BPA exposure. In the present study, BPA administration resulted in a 10.49% reduction in body weight, whereas concomitant NFZ treatment was associated with an 8.76% increase. These findings can be considered alongside those of Sharma et al. [53] who reported a 13% reduction in body weight following oral BPA administration at 50 mg/kg/day for 28 days in adult male rats. Furthermore, body weight progression in the NFZ-alone group was broadly comparable to that in the control group.

The standardized heatmap provides a descriptive overview of the treatment response and demonstrates that BPA altered several related domains of cardiac physiology, including myocardial injury, oxidative balance, inflammatory signaling, and antioxidant defense. The opposing visual patterns of injury-associated and antioxidant-related parameters are consistent with a broad BPA-associated cardiotoxic phenotype. The movement of the BPA + NFZ profile toward the control group suggests attenuation of these BPA-related abnormalities by NFZ.

Limitations

Despite these findings, several limitations should be considered. The experiments were performed exclusively in male rats, and thus the potential influence of sex differences and the applicability of the findings to human cardiovascular disease remain to be established. In addition, only a single dose of NFZ was investigated, precluding assessment of a dose–response relationship and preventing determination of whether the observed cardioprotective effects are dose dependent. The absence of functional assessments of cardiac performance, such as echocardiography or hemodynamic measurements, also limits interpretation of the physiological relevance of the observed molecular and histopathological changes. Although myocardial collagen deposition was quantified histologically, fibrosis-related markers, including collagen I and collagen III, were not assessed at the molecular level, limiting further characterization of ECM remodeling. Furthermore, although the coordinated changes in TLR-4/NF-κB and SIRT1/Nrf2/HO-1 signaling were associated with the protective effects of NFZ, the present study did not employ pathway-specific pharmacological inhibition or genetic silencing. Similarly, the roles of HIF-1α and TXNRD1 were evaluated as associated molecular responses rather than independently validated functional mediators. Future investigations incorporating multiple NFZ dose levels and dose-response analyses, functional cardiac evaluation, molecular assessment of fibrosis, and targeted mechanistic approaches will be valuable for further determining the translational relevance of NFZ in BPA-induced myocardial injury.

5. Conclusions

This study provides preclinical evidence that NFZ ameliorates BPA-induced cardiotoxicity in rats, as demonstrated by improvements in circulating cardiac injury biomarkers, myocardial oxidative and inflammatory status, histopathological alterations, and associated molecular changes. This cardioprotective effect was accompanied by reduced TLR-4/NF-κB-related inflammatory signaling and preservation of the SIRT1/Nrf2/HO-1 antioxidant pathway, together with restoration of HIF-1α and TXNRD1 expression. These findings support an association between modulation of these molecular pathways and the protective effects of NFZ against BPA-induced myocardial injury. Our findings suggest that NFZ may represent a promising protective agent against cardiotoxicity associated with exposure to BPA. Further preclinical studies are needed to assess its efficacy in preventing or reversing BPA-induced cardiac dysfunction in more complex models, such as those incorporating co-morbidities relevant to human cardiovascular disease. Clinical trials would ultimately be required to translate these findings into human therapeutic applications. Moreover, exploring potential synergistic effects of NFZ with other cardioprotective agents could lead to more effective combination therapies. The identification of NFZ as a modulator of SIRT1/Nrf2/HO-1 and TLR-4/NF-κB pathways also suggests its potential utility in other inflammatory and oxidative stress-related diseases beyond cardiotoxicity.

Availability of Data and Materials

The datasets used and analyzed during the current study are available from the corresponding author on reasonable request.

Author Contributions

AMM, RNA, and EHMH designed the research study; RNA, EHMH, AB, AAA, and AMM performed the research; RNA, EHMH, AB, AAA, SMA, AHB, MAE, and AMM collected and analyzed the data. AMM and RNA have been involved in drafting the manuscript and all authors have been involved in revising it critically for important intellectual content. All authors contributed to editorial changes in the manuscript. All authors read and approved the final manuscript. All authors have participated sufficiently in the work and agreed to be accountable for all aspects of the work.

Ethics Approval and Consent to Participate

All experimental procedures were conducted in accordance with the National Institutes of Health Guide for the Care and Use of Laboratory Animals (NIH Publication No. 85-23, revised 1996) and were approved by the Institutional Animal Ethics Committee of Al-Azhar University (Approval No. AZ-AS\PH-REC\12\26). The study was carried out in accordance with the ARRIVE guidelines.

Acknowledgment

The authors extend their appreciation to the Ongoing Research Funding Program (ORF-2026-1785), King Saud University, Riyadh, Saudi Arabia.

Funding

This work was supported by the Ongoing Research Funding Program (ORF-2026-1785), King Saud University, Riyadh, Saudi Arabia.

Conflicts of Interest

The authors declare no conflicts of interest.

Supplementary Material

Supplementary material associated with this article can be found, in the online version, at https://doi.org/10.31083/FBL57166.

References

[1] Hahladakis JN, Iacovidou E, Gerassimidou S. An overview of the occurrence, fate, and human risks of the bisphenol-A present in plastic materials, components, and products. Integrated En-

vironmental Assessment and Management. 2023; 19: 45–62. https://doi.org/10.1002/ieam.4611
[2] Vilarinho F, Sendón R, van der Kellen A, Vaz MF, Silva AS. Bisphenol A in food as a result of its migration from food packaging. Trends in Food Science & Technology. 2019; 91: 33–65. https://doi.org/10.1016/j.tifs.2019.06.012
[3] Rochester JR. Bisphenol A and human health: a review of the literature. Reproductive Toxicology (Elmsford, N.Y.). 2013; 42: 132–155. https://doi.org/10.1016/j.reprotox.2013.08.008
[4] Hu M, Zhang Z, Zhang Y, Zhan M, Qu W, He G, et al. Development of human dermal PBPK models for the bisphenols BPA, BPS, BPF, and BPAF with parallel-layered skin compartment: Basing on dermal administration studies in humans. The Science of the Total Environment. 2023; 868: 161639. https://doi.org/10.1016/j.scitotenv.2023.161639
[5] Sasso AF, Pirow R, Andra SS, Church R, Nachman RM, Linke S, et al. Pharmacokinetics of bisphenol A in humans following dermal administration. Environment International. 2020; 144: 106031. https://doi.org/10.1016/j.envint.2020.106031
[6] Kawa IA, Akbar Masood, Fatima Q, Mir SA, Jeelani H, Manzoor S, et al. Endocrine disrupting chemical Bisphenol A and its potential effects on female health. Diabetes & Metabolic Syndrome. 2021; 15: 803–811. https://doi.org/10.1016/j.dsx.2021.03.031
[7] Wang M, Rang O, Liu F, Xia W, Li Y, Zhang Y, et al. A systematic review of metabolomics biomarkers for Bisphenol A exposure. Metabolomics: Official Journal of the Metabolomic Society. 2018; 14: 45. https://doi.org/10.1007/s11306-018-1342-z
[8] Gao R, Ma J, Chen X, Jiang Z, Zhang C, An J, et al. Bisphenol A disrupts renal metabolism via MAPK-mediated steroid hormone dysregulation identified by transcriptomic and metabolomic analyses. Scientific Reports. 2025; 15: 36334. https://doi.org/10.1038/s41598-025-20141-3
[9] Gao X, Wang HS. Impact of bisphenol a on the cardiovascular system - epidemiological and experimental evidence and molecular mechanisms. International Journal of Environmental Research and Public Health. 2014; 11: 8399–8413. https://doi.org/10.3390/ijerph110808399
[10] Fonseca MI, Lorigo M, Cairrao E. Endocrine-Disrupting Effects of Bisphenol A on the Cardiovascular System: A Review. Journal of Xenobiotics. 2022; 12: 181–213. https://doi.org/10.3390/jox12030015
[11] Han C, Hong YC. Bisphenol A, Hypertension, and Cardiovascular Diseases: Epidemiological, Laboratory, and Clinical Trial Evidence. Current Hypertension Reports. 2016; 18: 11. https://doi.org/10.1007/s11906-015-0617-2
[12] Gao X, Liang Q, Chen Y, Wang HS. Molecular mechanisms underlying the rapid arrhythmogenic action of bisphenol A in female rat hearts. Endocrinology. 2013; 154: 4607–4617. https://doi.org/10.1210/en.2013-1737
[13] Badawy MM, Elsherbiny MM, Elshopakey GE, Elsayyad AE, Abd-El-Same'e El-Kattan M, Hamama MG, et al. Potential Effects of Bisphenol A on the Heart and Coronary Artery of Adult Male Rats and the Possible Role of L-Carnitine. Journal of Toxicology. 2022; 2022: 7760594. https://doi.org/10.1155/2022/7760594
[14] Posnack NG, Brooks D, Chandra A, Jaimes R, Sarvazyan N, Kay M. Physiological response of cardiac tissue to bisphenol A: alterations in ventricular pressure and contractility. American Journal of Physiology. Heart and Circulatory Physiology. 2015; 309: H267–H275. https://doi.org/10.1152/ajpheart.00272.2015
[15] Gassman NR. Induction of oxidative stress by bisphenol A and its pleiotropic effects. Environmental and Molecular Mutagenesis. 2017; 58: 60–71. https://doi.org/10.1002/em.22072
[16] Wang K, Zhao Z, Ji W. Bisphenol A induces apoptosis, oxidative stress and inflammatory response in colon and liver of mice in a mitochondria-dependent manner. Biomedicine & Pharmacotherapy = Biomedecine & Pharmacotherapie. 2019; 117: 109182. https://doi.org/10.1016/j.biopha.2019.109182
[17] Chandimali N, Bak SG, Park EH, Lim HJ, Won YS, Kim EK, et al. Free radicals and their impact on health and antioxidant defenses: a review. Cell Death Discovery. 2025; 11: 19. https://doi.org/10.1038/s41420-024-02278-8
[18] Asehnoune K, Strassheim D, Mitra S, Kim JY, Abraham E. Involvement of reactive oxygen species in Toll-like receptor 4-dependent activation of NF-kappa B. Journal of Immunology (Baltimore, Md.: 1950). 2004; 172: 2522–2529. https://doi.org/10.4049/jimmunol.172.4.2522
[19] Karunarathne WAHM, Molagoda IMN, Choi YH, Park SR, Lee S, Kim GY. Bisphenol A: A potential Toll-like receptor 4/myeloid differentiation factor 2 complex agonist. Environmental Pollution (Barking, Essex: 1987). 2021; 278: 116829. https://doi.org/10.1016/j.envpol.2021.116829
[20] Yang Y, Lv J, Jiang S, Ma Z, Wang D, Hu W, et al. The emerging role of Toll-like receptor 4 in myocardial inflammation. Cell Death & Disease. 2016; 7: e2234. https://doi.org/10.1038/cddis.2016.140
[21] Satta S, Mahmoud AM, Wilkinson FL, Yvonne Alexander M, White SJ. The Role of Nrf2 in Cardiovascular Function and Disease. Oxidative Medicine and Cellular Longevity. 2017; 2017: 9237263. https://doi.org/10.1155/2017/9237263
[22] Yang Y, Liu Y, Wang Y, Chao Y, Zhang J, Jia Y, et al. Regulation of SIRT1 and Its Roles in Inflammation. Frontiers in Immunology. 2022; 13: 831168. https://doi.org/10.3389/fimmu.2022.831168
[23] Xu JJ, Cui J, Lin Q, Chen XY, Zhang J, Gao EH, et al. Protection of the enhanced Nrf2 deacetylation and its downstream transcriptional activity by SIRT1 in myocardial ischemia/reperfusion injury. International Journal of Cardiology. 2021; 342: 82–93. https://doi.org/10.1016/j.ijcard.2021.08.007
[24] Yeung F, Hoberg JE, Ramsey CS, Keller MD, Jones DR, Frye RA, et al. Modulation of NF-kappaB-dependent transcription and cell survival by the SIRT1 deacetylase. The EMBO Journal. 2004; 23: 2369–2380. https://doi.org/10.1038/sj.emboj.7600244
[25] Joo HY, Yun M, Jeong J, Park ER, Shin HJ, Woo SR, et al. SIRT1 deacetylates and stabilizes hypoxia-inducible factor-1α (HIF-1α) via direct interactions during hypoxia. Biochemical and Biophysical Research Communications. 2015; 462: 294–300. https://doi.org/10.1016/j.bbrc.2015.04.119
[26] Tekin D, Dursun AD, Xi L. Hypoxia inducible factor 1 (HIF-1) and cardioprotection. Acta Pharmacologica Sinica. 2010; 31: 1085–1094. https://doi.org/10.1038/aps.2010.132
[27] Rahman MA, Rahaman KA, Harrath AH, Al-Zharani M, Jalouli M. Hypoxia-inducible factor-1α in cardiovascular disease, mechanistic insights, pathophysiological roles, and therapeutic targeting strategies. Biochemical Pharmacology. 2026; 246: 117753. https://doi.org/10.1016/j.bcp.2026.117753
[28] Rose AH, Hoffmann PR. Selenoproteins and cardiovascular stress. Thrombosis and Haemostasis. 2015; 113: 494–504. https://doi.org/10.1160/TH14-07-0603
[29] Althagafy HS, El-Aziz MKA, Ibrahim IM, Abd-Alhameed EK, Hassanein EHM. Pharmacological updates of nifuroxazide: Promising preclinical effects and the underlying molecular mechanisms. European Journal of Pharmacology. 2023; 951: 175776. https://doi.org/10.1016/j.ejphar.2023.175776
[30] Alzoghaibi MA, Hassanein EHM, Alotaibi MF, Alzoghaibi AM, Althagafy HS, Qebesy HS, et al. Nifuroxazide attenuates bisphenol A-induced male reproductive toxicity by modulating oxidative stress, inflammation, and Nrf2/HO-1 and necroptosis pathways. Tissue & Cell. 2026; 99: 103235. https://doi.org/10.1016/j.tice.2025.103235

[31] Ali FEM, M Elfiky M, Fadda WA, Ali HS, Mahmoud AR, Mohammedsaleh ZM, et al. Regulation of IL-6/STAT-3/Wnt axis by nifuroxazide dampens colon ulcer in acetic acid-induced ulcerative colitis model: Novel mechanistic insight. Life Sciences. 2021; 276: 119433. https://doi.org/10.1016/j.lfs.2021.119433
[32] Wisniewski P, Romano RM, Kizys MML, Oliveira KC, Kasamatsu T, Giannocco G, et al. Adult exposure to bisphenol A (BPA) in Wistar rats reduces sperm quality with disruption of the hypothalamic-pituitary-testicular axis. Toxicology. 2015; 329: 1–9. https://doi.org/10.1016/j.tox.2015.01.002
[33] Abraham NG, Lutton JD, Levere RD. Heme metabolism and erythropoiesis in abnormal iron states: role of delta-aminolevulinic acid synthase and heme oxygenase. Experimental Hematology. 1985; 13: 838–843.
[34] Livak KJ, Schmittgen TD. Analysis of relative gene expression data using real-time quantitative PCR and the 2(-Delta Delta C(T)) Method. Methods (San Diego, Calif.). 2001; 25: 402–408. https://doi.org/10.1006/meth.2001.1262
[35] Dallakyan S, Olson AJ. Small-molecule library screening by docking with PyRx. Methods in Molecular Biology (Clifton, N.J.). 2015; 1263: 243–250. https://doi.org/10.1007/978-1-4939-2269-7_19
[36] Wallace AC, Laskowski RA, Thornton JM. LIGPLOT: a program to generate schematic diagrams of protein-ligand interactions. Protein Engineering. 1995; 8: 127–134. https://doi.org/10.1093/protein/8.2.127
[37] Abd-Alhameed EK, Azouz AA, Abo-Youssef AM, Ali FEM. The enteroprotective effect of nifuroxazide against methotrexate-induced intestinal injury involves co-activation of PPAR-γ, SIRT1, Nrf2, and suppression of NF-κB and JAK1/STAT3 signals. International Immunopharmacology. 2024; 127: 111298. https://doi.org/10.1016/j.intimp.2023.111298
[38] Wallace KB, Hausner E, Herman E, Holt GD, MacGregor JT, Metz AL, et al. Serum troponins as biomarkers of drug-induced cardiac toxicity. Toxicologic Pathology. 2004; 32: 106–121. https://doi.org/10.1080/01926230490261302
[39] Preus M, Bhargava AS, Khater AE, Günzel P. Diagnostic value of serum creatine kinase and lactate dehydrogenase isoenzyme determinations for monitoring early cardiac damage in rats. Toxicology Letters. 1988; 42: 225–233. https://doi.org/10.1016/0378-4274(88)90081-1
[40] Garg P, Morris P, Fazlanie AL, Vijayan S, Dancso B, Dastidar AG, et al. Cardiac biomarkers of acute coronary syndrome: from history to high-sensitivity cardiac troponin. Internal and Emergency Medicine. 2017; 12: 147–155. https://doi.org/10.1007/s11739-017-1612-1
[41] Valokola MG, Karimi G, Razavi BM, Kianfar M, Jafarian AH, Jaafari MR, et al. The protective activity of nanomicelle curcumin in bisphenol A-induced cardiotoxicity following subacute exposure in rats. Environmental Toxicology. 2019; 34: 319–329. https://doi.org/10.1002/tox.22687
[42] Eweda SM, Newairy ASA, Abdou HM, Gaber AS. Bisphenol A-induced oxidative damage in the hepatic and cardiac tissues of rats: The modulatory role of sesame lignans. Experimental and Therapeutic Medicine. 2020; 19: 33–44. https://doi.org/10.3892/etm.2019.8193
[43] Frangogiannis NG. Cardiac fibrosis. Cardiovascular Research. 2021; 117: 1450–1488. https://doi.org/10.1093/cvr/cvaa324
[44] Belcher SM, Gear RB, Kendig EL. Bisphenol A alters autonomic tone and extracellular matrix structure and induces sex-specific effects on cardiovascular function in male and female CD-1 mice. Endocrinology. 2015; 156: 882–895. https://doi.org/10.1210/en.2014-1847
[45] Al-Abbas NS, Shaer NA. Nifuroxazide attenuated 5-fluorouracil-induced cardiac intoxication by regulating NLRP3/STAT-3, PPAR-γ, and apoptosis signals. Human & Experimental Toxicology. 2025; 44: 9603271251371245. https://doi.org/10.1177/09603271251371245
[46] Wang B, Wang Y, Zhang J, Hu C, Jiang J, Li Y, et al. ROS-induced lipid peroxidation modulates cell death outcome: mechanisms behind apoptosis, autophagy, and ferroptosis. Archives of Toxicology. 2023; 97: 1439–1451. https://doi.org/10.1007/s00204-023-03476-6
[47] Alruhaimi RS, Alotaibi RN, Alnasser SM, Al-Thubiani WS, Aldawood N, Hassanein EHM, et al. Carbocisteine mitigates bisphenol A-mediated renal injury by modulating oxidative stress, Keap1/Nrf2/HO-1 pathway, endoplasmic reticulum stress, and inflammation. Toxicological Research. 2026. https://doi.org/10.1007/s43188-026-00366-8
[48] Alzoghaibi MA, Hassanein EHM, Alotaibi MF, Alzoghaibi AM, Althagafy HS, Qebesy HS, et al. Modulation of Redox Homeostasis, Inflammation, and Necroptosis by Carbocisteine Protects Against Bisphenol A-Induced Male Reproductive Toxicity. Bratislava Medical Journal. 2026; 127: 2155–2173. https://doi.org/10.1007/s44411-026-00621-2
[49] Yin K, Sun X, Zheng Y, Zhang W, Lin H. Bisphenol A exacerbates selenium deficiency-induced pyroptosis via the NF-κB/NLRP3/Caspase-1 pathway in chicken trachea. Comparative Biochemistry and Physiology. Toxicology & Pharmacology: CBP. 2023; 263: 109488. https://doi.org/10.1016/j.cbpc.2022.109488
[50] Said E, Zaitone SA, Eldosoky M, Elsherbiny NM. Nifuroxazide, a STAT3 inhibitor, mitigates inflammatory burden and protects against diabetes-induced nephropathy in rats. Chemico-biological Interactions. 2018; 281: 111–120. https://doi.org/10.1016/j.cbi.2017.12.030
[51] Choy MK, Movassagh M, Siggens L, Vujic A, Goddard M, Sánchez A, et al. High-throughput sequencing identifies STAT3 as the DNA-associated factor for p53-NF-kappaB-complex-dependent gene expression in human heart failure. Genome Medicine. 2010; 2: 37. https://doi.org/10.1186/gm158
[52] Gozzelino R, Jeney V, Soares MP. Mechanisms of cell protection by heme oxygenase-1. Annual Review of Pharmacology and Toxicology. 2010; 50: 323–354. https://doi.org/10.1146/annurev.pharmtox.010909.105600
[53] Sharma P, Mandal MB, Katiyar R, Singh SP, Birla H. A Comparative Study of Effects of 28-Day Exposure of Bisphenol A and Bisphenol S on Body Weight Changes, Organ Histology, and Relative Organ Weight. International Journal of Applied & Basic Medical Research. 2021; 11: 214–220. https://doi.org/10.4103/ijabmr.IJABMR_663_20